View metadata, citation and similar papers at core.ac.uk
brought to you by CORE
provided by Caltech Authors - Main

The Astronomical Journal, 160:193 (8pp), 2020 October
https://doi.org/10.3847/1538-3881/abb3bd
© 2020. The American Astronomical Society. All rights reserved.

The TESS-Keck Survey. III. A Stellar Obliquity Measurement of TOI-1726 c

Fei Dai[1], Arpita Roy[2], Benjamin Fulton[3], Paul Robertson[4], Lea Hirsch[5], Howard Isaacson[6], Simon Albrecht[7], Andrew W. Mann[8], Martti H. Kristiansen[9,10], Natalie M. Batalha[11], Corey Beard[4], Aida Behmard[1], Ashley Chontos[12,26], Ian J. M. Crossfield[13], Paul A. Dalba[14,27], Courtney Dressing[6], Steven Giacalone[6], Michelle Hill[14], Andrew W. Howard[15], Daniel Huber[12], Stephen R. Kane[14], Molly Kosiarek[11], Jack Lubin[4], Andrew Mayo[6], Teo Mocnik[16], Joseph M. Akana Murphy[11,26], Erik A. Petigura[17], Lee Rosenthal[2], Ryan A. Rubenzahl[2,26], Nicholas Scarsdale[11], Lauren M. Weiss[12], Judah Van Zandt[17], George R. Ricker[18], Roland Vanderspek[18], David W. Latham[19], Sara Seager[18,20,21], Joshua N. Winn[22], Jon M. Jenkins[23], Douglas A. Caldwell[23,24], David Charbonneau[19], Tansu Daylan[25,28], Maximilian N. Günther[25,29], Edward Morgan[21], Samuel N. Quinn[19], Mark E. Rose[23], and Jeffrey C. Smith[23,24]

[1] Division of Geological and Planetary Sciences, California Institute of Technology, 1200 E. California Blvd., Pasadena, CA 91125, USA; fdai@caltech.edu
[2] Department of Astronomy, California Institute of Technology, Pasadena, CA 91125, USA
[3] NASA Exoplanet Science Institute/Caltech-IPAC, MC 314-6, 1200 E. California Blvd., Pasadena, CA 91125, USA
[4] Department of Physics & Astronomy, The University of California, Irvine, Irvine, CA 92697, USA
[5] Kavli Institute for Particle Astrophysics and Cosmology, Stanford University, Stanford, CA, USA
[6] 501 Campbell Hall, University of California at Berkeley, Berkeley, CA 94720, USA
[7] Stellar Astrophysics Centre, Department of Physics and Astronomy, Aarhus University, Ny Munkegade 120, DK-8000 Aarhus C, Denmark
[8] Department of Physics and Astronomy, The University of North Carolina at Chapel Hill, Chapel Hill, NC 27599, USA
[9] Brorfelde Observatory, Observator Gyldenkernes Vej 7, DK-4340 Tølløse, Denmark
[10] DTU Space, National Space Institute, Technical University of Denmark, Elektrovej 327, DK-2800 Lyngby, Denmark
[11] Department of Astronomy and Astrophysics, University of California, Santa Cruz, CA 95060, USA
[12] Institute for Astronomy, University of Hawai'i, 2680 Woodlawn Dr., Honolulu, HI 96822, USA
[13] Department of Physics and Astronomy, University of Kansas, Lawrence, KS, USA
[14] Department of Earth and Planetary Sciences, University of California, Riverside, CA 92521, USA
[15] California Institute of Technology, Pasadena, CA 91125, USA
[16] Gemini Observatory Northern Operations, 670 N. A'ohoku Pl., Hilo, HI 96720, USA
[17] Department of Physics & Astronomy, University of California Los Angeles, Los Angeles, CA 90095, USA
[18] Department of Physics and Kavli Institute for Astrophysics and Space Research, Massachusetts Institute of Technology, Cambridge, MA 02139, USA
[19] Center for Astrophysics|Harvard & Smithsonian, 60 Garden St., Cambridge, MA 02138, USA
[20] Department of Earth, Atmospheric and Planetary Sciences, Massachusetts Institute of Technology, Cambridge, MA 02139, USA
[21] Department of Aeronautics and Astronautics, MIT, 77 Massachusetts Ave., Cambridge, MA 02139, USA
[22] Department of Astrophysical Sciences, Princeton University, 4 Ivy Ln., Princeton, NJ 08544, USA
[23] NASA Ames Research Center, Moffett Field, CA 94035, USA
[24] SETI Institute, Mountain View, CA, USA
[25] Department of Physics and Kavli Institute for Astrophysics and Space Research, Massachusetts Institute of Technology, 70 Vassar St., Cambridge, MA 02139, USA

Received 2020 May 6; revised 2020 August 19; accepted 2020 August 27; published 2020 September 30

Abstract

We report the measurement of a spectroscopic transit of TOI-1726c, one of two planets transiting a G-type star with $V = 6.9$ in the Ursa Major Moving Group (~400 Myr). With a precise age constraint from cluster membership, TOI-1726 provides a great opportunity to test various obliquity excitation scenarios that operate on different timescales. By modeling the Rossiter–McLaughlin (RM) effect, we derived a sky-projected obliquity of $-1^{+35}_{-32}{}^{\circ}$. This result rules out a polar/retrograde orbit and is consistent with an aligned orbit for planet c. Considering the previously reported, similarly prograde RM measurement of planet b and the transiting nature of both planets, TOI-1726 tentatively conforms to the overall picture that compact multitransiting planetary systems tend to have coplanar, likely aligned orbits. TOI-1726 is also a great atmospheric target for understanding differential atmospheric loss of sub-Neptune planets (planet b 2.2 $R_\oplus$ and c 2.7 $R_\oplus$ both likely underwent photoevaporation). The coplanar geometry points to a dynamically cold history of the system that simplifies any future modeling of atmospheric escape.

Unified Astronomy Thesaurus concepts: Exoplanet dynamics (490); Exoplanet formation (492)

1. Introduction

The stellar obliquity is the angle between the rotation axis of the host star and the normal of the orbital plane of its planet. While the planets in the solar system are well aligned with the Sun (obliquity $\lesssim 7°$), many of the known exoplanets have polar or even retrograde orbits (e.g., Sanchis-Ojeda et al. 2013; Dalal et al. 2019). These spin–orbit misalignments are often interpreted as signposts of a dynamically hot formation or evolution history. Various mechanisms have been proposed to be responsible for tilting the orbits of planets. Many of these mechanisms operate on different timescales: primordial disk misalignment during the disk-hosting stage ($\lesssim$ 3 Myr; e.g., Lai et al. 2011; Batygin 2012), nodal procession induced by an inclined companion (~3.5 Myr for HAT-P-11b; Yee et al.

[26] NSF Graduate Research Fellow.
[27] NSF Astronomy and Astrophysics Postdoctoral Fellow.
[28] Kavli Fellow.
[29] Juan Carlos Torres Fellow.

2018), the Kozai–Lidov mechanism operating on a wide range of timescales, 10^4–10^8 yr, depending on the system configuration (e.g., Fabrycky & Tremaine 2007), and secular chaos between longer-period giant planets can happen in 10^7–10^8 yr (e.g., Wu & Lithwick 2011). A sample of obliquity measurements spanning a range of precise host star ages will help us distinguish these orbit-tilting mechanisms.

Precise stellar ages for main-sequence stars are hard to come by, particularly for later-type stars which barely evolve over a Hubble time. Our best age constraints come from establishing the cluster membership of a planet host so that the ensemble study of kinematics, stellar activity, Li abundance, gyrochronology, and isochronal fitting of other stars in the same cluster can firmly pin down the stellar age. So far there are about a dozen planet hosts found in young clusters (e.g., David et al. 2016; Mann et al. 2016). They are crucial for our understanding of various aspects of planet formation and evolution. TOI-1726 is a G-type star in the Ursa Major Moving Group (414 ± 23 Myr; Jones et al. 2015) that hosts two transiting sub-Neptune planets with 2.2 and 2.7 $R_\odot$ on 7 and 20 day orbits (Mann et al. 2020). With a V-band magnitude of 6.9 and a projected rotational velocity $v\sin i$ of $\sim$7 km s^{-1}, TOI-1726 provides a rare opportunity to measure the stellar obliquity of a young sub-Neptune planet. In this work, we discuss a new measurement of the stellar obliquity of planet c.

This paper is structured as follows. In Section 2 we present the spectroscopic measurements of the TOI-1726. Section 3 describes the constraints on the stellar parameters using both spectroscopy and Gaia information. In Section 4, we present a joint analysis of the Transiting Exoplanet Survey Satellite (TESS) light curve and the Rossiter–McLaughlin (RM) effect to measure the stellar obliquity of TOI-1726c. Section 5 discusses the implication of our finding.

2. Spectroscopic Measurement

We obtained 49 spectra of TOI-1726 on the night of UTC 2020 February 26, spanning a transit of TOI-1726c. We used the Automated Planet Finder (APF; Vogt et al. 2014) at the Lick Observatory. The spectra were obtained with an iodine cell whose dense forest of molecular lines provide both the wavelength solution and a means of determining the line-spread function. The spectral resolution was $\sim$100,000. We obtained consecutive 10 minute exposures that enabled a median signal-to-noise ratio (S/N) of 145 per reduced pixel near 5500 Å. The iodine method for determining precise radial velocities requires a template spectrum of the star with a high S/N. A template spectrum should have been obtained with the APF. However, due to weather conditions and scheduling constraints, we had to secure a high S/N template of TOI-1726 on the High Resolution Echelle Spectrometer (HIRES) on the 10 m Keck I telescope on the night of UT 2020 March 10. APF and HIRES have similar instrumental designs (Vogt et al. 1994, 2014). Moreover, we explicitly deconvolved the different instrumental profiles from the template spectra in our Doppler pipeline (Howard et al. 2010), therefore the high S/N, iodine-free HIRES spectrum should serve adequately as the template spectrum for reducing the APF data set. More details of our forward-modeling Doppler pipeline are described in Howard et al. (2010). The radial velocities and uncertainties are plotted in Figure 1 and reported in Table 1.

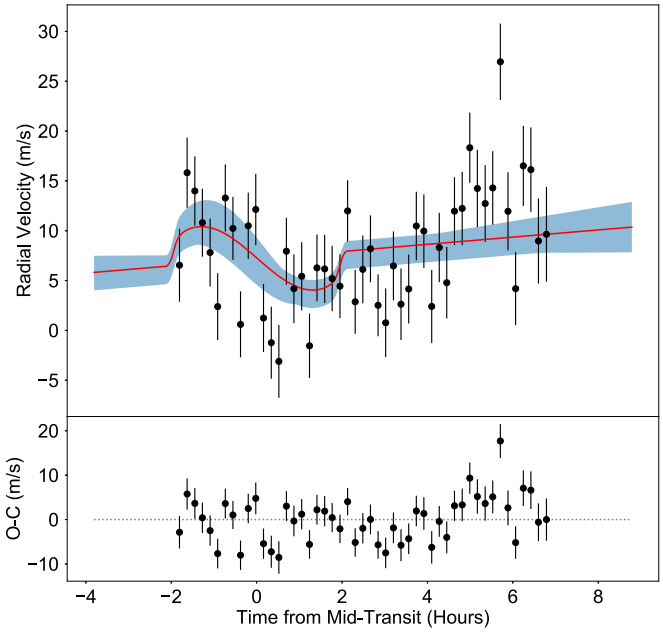

Figure 1. The measured radial velocities during the transit of TOI-1726c. The red line is the best-fit model; the blue shaded region represents the 68% confidence region from the posterior distribution. The data suggest a stellar obliquity of -1^{+35}_{-32}° that favors a prograde, and likely aligned orbit for TOI-1726c. Visually, there are also hints of a red noise component toward the end of observation. We investigated the source of this red noise component with a line profile analysis and its effect on the obliquity measurement with a Prayer's Beads analysis in Section 4.

3. Stellar Parameters

We constrained the spectroscopic parameters ($T_{\rm eff}$, log g, and [Fe/H]) of TOI-1726 using the iodine-free spectra from Keck/HIRES and the SpecMatch pipeline[30] (Petigura et al. 2017). In short, SpecMatch models observed optical spectra with interpolated model spectra from the precomputed grid (Coelho et al. 2005) of discrete $T_{\rm eff}$, [Fe/H], log g, and $v\sin i$ values. Line broadening effects from both rotation and macroturbulence are included by convolving the model spectra with the kernel described by Hirano et al. (2011). Instrumental broadening is modeled as a Gaussian function with an FWHM of 3.8 pixels, a value that provides a good match to the widths of telluric lines. We calculate the weighted average of the spectroscopic parameters of five $\sim$400 Å spectral segments. The final output spectroscopic parameters are corrected for known systematic effects from previous comparisons with standard stars. Particularly, SpecMatch systematically yields higher ($\sim$0.1 dex) surface gravity log g for earlier-type stars when compared with asteroseismic results of standard stars (Huber et al. 2013a). This effect is empirically corrected for with a scaling relation log $g(T_{\rm eff}$,[Fe/H]). See Petigura (2015) for details.

To derive the stellar parameters, we further make use of Gaia parallax information (Gaia Collaboration et al. 2018). We followed the procedure described in detail by Fulton & Petigura (2018). To summarize, we link the stellar effective temperature, the parallax measurement from Gaia, and the K-band magnitude (which is less affected by extinction) together with Stefan Boltzmann Law for an independent constraint on the radius of the star. In practice, we put in the priors on

[30] https://github.com/petigura/specmatch-syn

Table 1
Lick/APF Radial Velocities

Time (BJD)	Radial Velocity (m s^{-1})	Radial Velocity Unc. (m s^{-1})	S Index	S Unc.
2458905.618603	6.54	3.66	0.374	0.002
2458905.626056	15.82	3.52	0.381	0.002
2458905.633579	13.99	3.47	0.373	0.002
2458905.640951	10.81	3.41	0.372	0.002
2458905.648485	7.82	3.41	0.375	0.002
2458905.655846	2.39	3.35	0.377	0.002
2458905.663311	13.29	3.37	0.382	0.002
2458905.670752	10.23	3.17	0.385	0.002
2458905.678159	0.61	3.31	0.375	0.002
2458905.685705	10.49	3.33	0.384	0.002
2458905.693031	12.14	3.57	0.386	0.002
2458905.700588	1.24	3.41	0.389	0.002
2458905.708180	−1.23	3.61	0.381	0.002
2458905.715564	−3.11	3.65	0.382	0.002
2458905.722925	7.94	3.36	0.380	0.002
2458905.730262	4.18	3.45	0.383	0.002
2458905.737843	5.43	3.42	0.381	0.002
2458905.745470	−1.55	3.22	0.379	0.002
2458905.752749	6.28	3.35	0.385	0.002
2458905.760260	6.17	3.41	0.381	0.002
2458905.767575	5.20	3.28	0.381	0.002
2458905.775190	4.44	3.20	0.391	0.002
2458905.782655	11.99	3.08	0.380	0.002
2458905.790061	2.87	3.21	0.384	0.002
2458905.797492	6.12	3.40	0.384	0.002
2458905.804945	8.19	3.35	0.381	0.002
2458905.812386	2.52	3.11	0.379	0.002
2458905.819793	0.77	3.44	0.367	0.002
2458905.827362	6.47	3.46	0.391	0.002
2458905.834758	2.63	3.59	0.382	0.002
2458905.842257	4.15	3.46	0.378	0.002
2458905.849699	10.48	3.43	0.379	0.002
2458905.857059	9.96	3.69	0.381	0.002
2458905.864721	2.41	3.66	0.375	0.002
2458905.872093	8.32	3.48	0.380	0.002
2458905.879396	4.79	3.59	0.374	0.002
2458905.886930	11.96	3.41	0.380	0.002
2458905.894476	12.24	3.67	0.376	0.002
2458905.901883	18.33	3.53	0.384	0.002
2458905.909255	14.24	3.88	0.385	0.002
2458905.916893	12.73	3.85	0.382	0.002
2458905.924254	14.29	3.69	0.383	0.002
2458905.931707	26.95	3.83	0.387	0.002
2458905.939126	11.95	3.92	0.386	0.002
2458905.946590	4.19	3.66	0.394	0.002
2458905.954113	16.51	4.02	0.383	0.002
2458905.961497	16.13	4.24	0.388	0.002
2458905.968869	8.97	4.26	0.383	0.002
2458905.976681	9.64	4.76	0.391	0.002

spectroscopic parameters and the parallaxes into the Isoclassify package of Huber et al. (2017) which then compares these parameters with the MESA Isochrones & Stellar Tracks (MIST; Choi et al. 2016) to determine the posterior distribution of various stellar parameters. The results are summarized in Table 2.

4. Joint Light Curve and RM Analysis

TOI-1726 was observed by TESS (Ricker et al. 2014) in Sector 20 from UT 2019 December 24 to 2020 January 20. We downloaded the reduced light curve from the Mikulski Archive for Space Telescopes website.[31] We only kept data points with a Quality Flag of zero, i.e., those with no known problems.

Table 2
Stellar and Transit Parameters of Planet c

Parameter	Symbol	Posterior Distribution
Sky-projected obliquity (deg)	λ	-1^{+35}_{-32}
Projected stellar rotation (km s^{-1})	$v\sin i$	7.0 ± 1.0
Radial velocity offset (m s^{-1})	γ	$4.69^{+1.95}_{-1.98}$
Radial velocity trend (m s^{-1} day^{-1})	$\dot{\gamma}$	$19.4^{+8.5}_{-8.8}$
Planet/star radius ratio	$R_p/R_\star$	$0.02660^{+0.00082}_{-0.00074}$
Planetary radius ($R_\oplus$)	R_p	2.71 ± 0.14
Time of conjunction (BJD-2,457,000)	t_0	1844.0577 ± 0.0011
Impact parameter	b	0.50 ± 0.07
Scaled semimajor axis	$a/R_\star$	$38.0^{+1.7}_{-4.6}$
Orbital period (days)	P_{orb}	$20.5456^{+0.0016}_{-0.0019}$
Jitter (m s^{-1})	σ	$3.66^{+0.80}_{-0.75}$
Effective temperature (T_{eff})	K	5710 ± 100
Surface gravity (dex)	log g	4.6 ± 0.1
Metallicity (dex)	[Fe/H]	0.05 ± 0.05
Projected stellar rotation from spectroscopy (km s^{-1})	$v\sin i$	6.56 ± 1.0
Stellar mass ($M_\odot$)	$M_\star$	0.994 ± 0.036
Stellar radius ($R_\odot$)	$R_\star$	0.934 ± 0.019
Stellar density (g cm^{-3})	$\rho_\star$	1.72 ± 0.17
Rotation period (days)	P_{rot}	$6.36^{+0.75}_{-0.25}$

We started from the transit ephemerides reported by the TESS team. We first removed the data spanning the transits of both planet b and c from the light curve. This enabled us to measure the stellar rotation period of TOI-1726 by applying the Lomb–Scargle periodogram. We detected a strong rotational modulation at a period of $6.36^{+0.75}_{-0.25}$ days where the uncertainties are derived from the FWHM of the peak. As a consistency check, we calculated $v = 2\pi R_\star/P_{rot}$, the rotation period of $6.36^{+0.75}_{-0.25}$ days, and the stellar radius of $0.92 \pm -0.10\,R_\odot$ together give a rotational velocity v of $7.3^{+0.7}_{-1.0}$ km s^{-1}, which is consistent with the $v\sin i$ of 6.56 ± 1.0 km s^{-1} determined from the spectroscopic analysis alone. Using the procedure described in Masuda & Winn (2020), the orbital inclination of the host star is >45° at a 95% confidence level. This agreement of $v\sin i$ and v is supporting evidence for a prograde and perhaps well-aligned orbit of TOI-1726c, in addition to the analysis of the RM effect described later in the paper.

We then analyzed the in-transit light curve simultaneously with the RM effect. We isolated data taken within one transit duration of the transit midpoint. We used the `Batman` package (Kreidberg 2015) to model the transit light curves. We adopted a quadratic limb-darkening law, imposing Gaussian priors on the coefficients with medians taken from precomputed limb-darkening coefficients from `EXOFAST`[32] (Eastman et al. 2013) and with widths of 0.3. We put a prior on the mean stellar density based on the analysis in Section 3. We sampled P_{orb}, $R_p/R_\star$, and $a/R_\star$ uniformly in logarithmic space. We put a uniform prior on the impact parameter b [−1,1] and on the midtransit time (T_c). We assumed that both planets are on circular orbits. The current radial velocity data set (L. Hirsch et al. 2020, in preparation) only provides weak constraints on

[31] https://archive.stsci.edu
[32] https://astroutils.astronomy.ohio-state.edu/exofast/limbdark.shtml.

the orbital eccentricities and are consistent with being circular for both planets.

To model the RM effect, we followed the prescription of Hirano et al. (2011). The additional parameters are the sky-projected obliquity λ, the projected rotational velocity $v\sin i$, the radial velocity offset γ, and the local gradient of the offset $\dot{\gamma}$. We also included a jitter parameter to account for any additional astrophysical or instrumental noise. The likelihood function of the RM model was combined with the likelihood function of the transit model.

We sampled the posterior distribution using the Markov Chain Monte Carlo technique implemented in the *e*mcee code (Foreman-Mackey et al. 2013). We used 128 walkers and ran until the Gelman–Rubin convergence statistics dropped below 1.03. We first included a prior on the rotational modulation $v\sin i$ of $6.56 \pm 1.0\,\mathrm{km\ s^{-1}}$ from spectroscopic analysis in Section 3. The sky-projected obliquity has a posterior distribution of $-6^{+28}_{-25}{}^{\circ}$, i.e., favor a prograde and possibly an aligned orbit for planet c. The posterior distribution also favors a slightly higher $v\sin i$ of $7.0 \pm 1.0\,\mathrm{km\ s^{-1}}$. When we removed the prior on $v\sin i$ altogether, the data are consistent with a broader range of $v\sin i$ of $9.9^{+4.3}_{-3.4}\,\mathrm{km\ s^{-1}}$, while the posterior distribution of stellar obliquity also widened, $\lambda - 5^{+33}_{-26}{}^{\circ}$. Table 2 reports the summary of the posterior distribution for the key parameters.

5. Doppler Tomography and Red Noise Mitigation

We tried to look for the Doppler shadow of planet c in the subtle variation of the line profiles using the non-iodine part of the spectra (4000–5000 Å). Our analysis is similar to that of Albrecht et al. (2013). In short, we cleaned the spectrum from outliers with a 5σ clipping. We removed the continuum and blaze function with a polynomial fit to the 95% percentile flux level in each Echelle order. We cross correlated the individual spectrum with the best-fit SpecMatch spectrum before rotational/instrumental broadening is applied. We then subtracted the globally averaged line profile from the individual line profiles to extract the subtle variations that may be caused by the shadow of the transiting planet (Figure 2). However, given the small transit depth of the planet ($\sim$0.08%), we could not convincingly detect the shadow of the planet in the line profile residuals. Instead, the line profile residuals are dominated by patterns that are almost one order of magnitude larger in amplitude, roughly constant in velocity, and extend well beyond the transit duration. We suspect that these patterns were most likely produced by the change of the point-spread function due to instrumental effects or the emergence of stellar activity on TOI-1726. However, we do not have a physically motivated model to eliminate these effects.

Visual inspection of the residuals of the RM time series hint at the presence of a correlated noise component more noticeably starting at 4 hr after the midtransit of planet c (Figure 1). This coincided the onset of correlated noises in the radial velocity residuals (Figure 2) as well as an increase of the S index (Table 1). To assess how the presence of a correlated noise component might have affected the constraint on stellar obliquity, we performed a Prayer's Beads analysis. This is perhaps more worrisome as some of the line profile residual patterns happened during the transit of planet c (Figure 2). Our analysis is as follows. We first found the maximum likelihood model with the Levenberg–Marquardt method as implemented in PYTHON package LMFIT. We recorded the corresponding residuals and cyclically permuted the residuals before adding them back to the best-fit model. This generated a series of mock data sets that contain the same correlated noise component as the original data set. We found the maximum likelihood model for each mock data set. Focusing on the stellar obliquity, the resultant distribution of obliquity is $\lambda = -1^{+35}_{-32}{}^{\circ}$. This is a broader distribution compared to that from the white noise–only model in Section 4, but qualitatively these two models both favor a prograde, possibly aligned orbit for TOI-1726c.

6. Discussion

6.1. Obliquity of Multitransiting Systems

It has been noted in several previous works that the underlying orbital architectures of Kepler single-transiting (here we refer to the observed multiplicity, to be distinguished from planets that only transited host stars once during the time span of observation) and multitransiting systems may be different. Specifically, single-transiting systems seem to have a broader distribution of orbital eccentricities whereas multi-transiting systems mostly favor circular orbits (van Eylen & Albrecht 2015; Xie et al. 2016; Mills et al. 2019). In addition, Fang & Margot (2012) and Zhu et al. (2018) suggested that the mutual inclination dispersion is larger when the observed multiplicity of a planetary system is smaller. A plausible explanation of this architectural difference is the dynamical interaction between the sub-Neptune planets or that with a more distant giant planets. Zhu & Wu (2018) and Bryan et al. (2019) independently arrived at the conclusion that Kepler-like sub-Neptune planets are much more likely to have a cold Jupiter companion (>1 au) than randomly chosen stars (Cumming et al. 2008; Clanton & Gaudi 2014). Masuda et al. (2020) further showed that when the inner planetary system only has one transiting planet, its cold Jupiter is likely inclined by tens of degrees relative to the inner planetary system. The interpretation is that the dynamical interaction of an inclined cold Jupiter can stir up the initially coplanar planetary systems while exciting larger mutual inclinations and eccentricities. The single-transiting systems represent the dynamically hot subsample while the multitransiting systems are dynamically colder.

It will be interesting to see if the same architectural difference carries over to the stellar obliquity distribution. So far, there are about 150 obliquity measurements in the literature. The traditional RM effect is more easily detected for planets with larger radii and more frequent transits. As a result, the vast majority of existing measurements were performed for hot Jupiters or hot Neptunes. Intriguingly, it is often the case that these hot Jupiters and hot Neptunes are single-transiting planets with spin–orbit misalignments both of which hint at a dynamically hot past (Dong et al. 2018). On the other hand, multitransiting systems tend to display low obliquities (Albrecht et al. 2013). Unfortunately there are only $\sim$11 obliquity measurements obtained for multitransiting systems to date (see Figure 3). We note the most complete census of spin–orbit angle of multitransiting systems was done by Winn et al. (2017). They compared the projected rotational velocity $v\sin i$ and the rotational velocity $v = 2\pi R_\star/P_{\mathrm{rot}}$. If a system is grossly misaligned, $v\ \sin i$ would be much smaller than v. Winn et al. (2017) found that the majority of Kepler-like systems (systems with several sub-Neptune planets within 1 au) are well aligned with their host star. The six high-obliquity

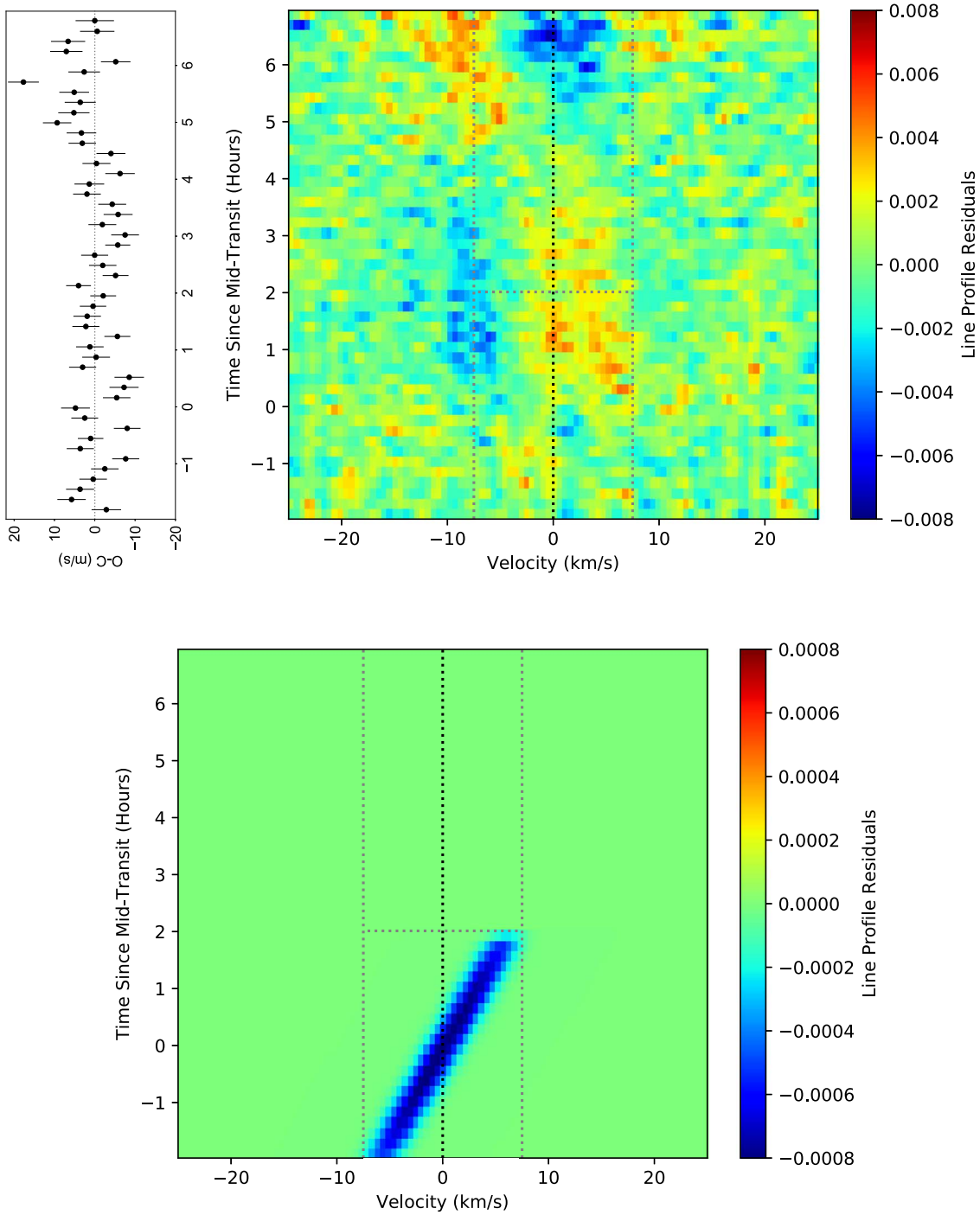

Figure 2. Top left: the residuals of the RM time series, same as Figure 1. Top right: the measured line profile residuals as a function of time and velocity. The vertical gray lines indicate the vsin*i* of the host star. The horizontal gray lines indicate the end of the transit t_{IV}. Some localized patterns can be seen which are likely due to a combination of stellar activity and instrumental drifts. Bottom: the simulated planetary shadow of TOI-1726c on a well-aligned orbit. The signal is about one order of magnitude lower than the uncertainties seen in the measurements (note the different color coding in these two panels) and remains undetected with the current measurement.

suspects Winn et al. (2017) identified were dominated by hot Jupiters. This result revealed a picture in which planets in multiplanet systems are generally well aligned, as one would expect from a cold dynamical history. Coming back to the multitransiting systems that have their stellar obliquities explicitly measured, most of these measurements were often obtained with alternative methods, rather than the RM effect, such as asteroseismology (e.g., Huber et al. 2013b) or spot-crossing anomalies (e.g., Sanchis-Ojeda et al. 2012). The results mostly yield well-aligned orbits. We note that the only exceptions are the polar orbit of HD 3167c (Dalal et al. 2019) and 50° inclined orbit of Kepler-56 b and c (Huber et al. 2013b). What kind of formation channel gave rise to misaligned multiplanet systems has been a topic of interest for the theorists (e.g., Li et al. 2014; Spalding & Batygin 2015). It will be interesting to see if these two systems are indeed rare occurrences. Our result on TOI-1726c is one crucial step toward enlarging that sample of multitransiting planetary

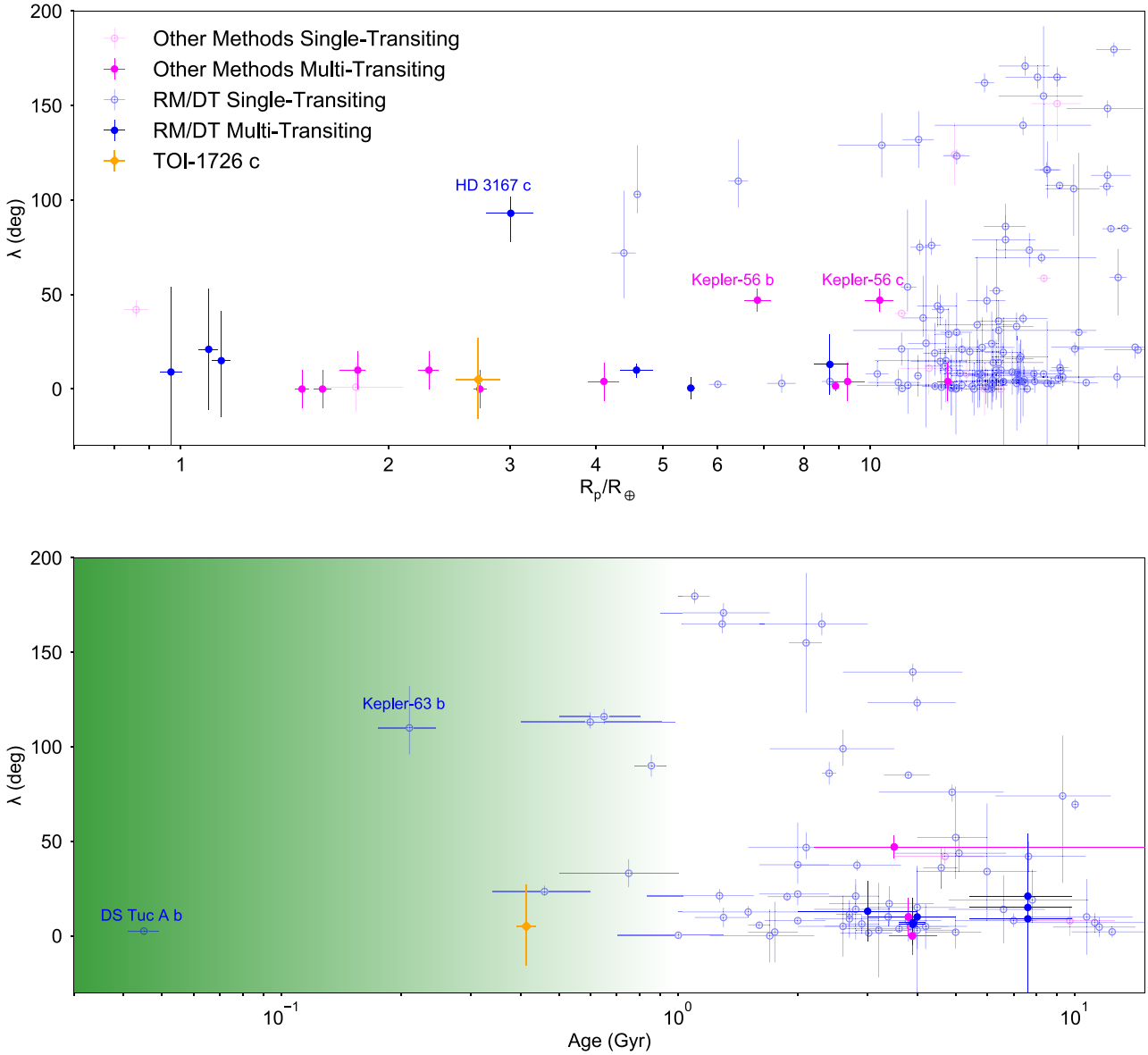

Figure 3. The projected stellar obliquity λ plotted against the planetary radius (upper) and stellar age (lower). The majority of stellar obliquity measurements are performed for single-transiting planets which are believed to have a dynamically hot history. We highlighted measurements of relatively unexplored multitransiting systems with filled symbols. TOI-1726 is a unique opportunity for obliquity measurement for multitransiting sub-Neptune planetary systems with a well-determined young age. The green shading in the lower panel qualitatively captures the magnitude of the high-energy radiation from the host star that is responsible for driving photoevaporation. These high-energy radiation dwindles with the first few hundred Myr: the timescale for future observations of TOI-1726 are poised to probe.

systems. Although the obliquity constraints on planet b and planet c individually are weak, $1^{+41}_{-43}{}^{\circ}$ (Mann et al. 2020) versus $-1^{+35}_{-32}{}^{\circ}$, the fact that both planets transit and the posterior distributions of obliquity both center at zero seems to favor a coplanar, likely aligned, dynamically quiet architecture for TOI-1726.

6.2. Obliquity in Time

As we mentioned briefly in the 1, many different theories have been offered to explain the observed diversity of stellar obliquities (e.g., Fabrycky & Tremaine 2007; Lai et al. 2011; Wu & Lithwick 2011; Batygin 2012; Yee et al. 2018). Since these theories operate on very different timescales, a potential way to test some of them is to obtain obliquity measurements for a sample of planets with well-determined ages. For example, if young planetary systems rarely display spin–orbit misalignment, it is reasonable to say that the orbit-tilting mechanisms that only operate during the disk-hosting stage (e.g., Lai et al. 2011; Batygin 2012) cannot be the dominant channel to generate spin–orbit misalignment. The cluster membership of TOI-1726 (Mann et al. 2020) provides a firm and precise age estimate for the host star. In Figure 3, we plotted all obliquity measurements for systems with better than 20% age estimates. TOI-1726c is the third youngest planet with obliquity measurement. Moreover TOI-1726c is a sub-Neptune which is the common outcome of planet formation as revealed by Kepler (Petigura et al. 2013). However, there are very few obliquity measurements for the sub-Neptunes (Figure 3).

6.3. A Great System for Studying Atmospheric Losses

The bimodal radius distribution and the presence of the so-called "hot Neptune desert" both suggest that atmospheric loss

from sub-Neptune planets is a common if not ubiquitous phenomena (Fulton et al. 2017). TOI-1726 is a great system for a study of atmospheric loss. The star is 400 Myr old, which is comparable to the timescale where high-energy radiation from the host star begins to diminish (Ribas et al. 2005) and the photoevaporation starts to come to a conclusion (see Figure 3). Moreover, the system contains two sub-Neptune planets whose low surface gravity make them the planets most amenable to photoevaporation (Wang & Dai 2018). The two planets are suited to comparative study since they orbit around the same host star. In other words, the planets are bathed in the same high-energy radiation environment except for a difference in orbital distance. Any difference in the outcome of atmospheric loss has to come from the different planetary parameters, e.g., orbital period, planetary mass, etc. The prograde and coplanar orbits of both planet b (Mann et al. 2020) and planet c together disfavor a violent event such as high-eccentricity migration or giant impact collision that would have disrupted the planets' coplanarity and complicated the evolution of the atmospheres. We also note that there is no compelling evidence for a cold Jupiter that may generate dynamical instability of the inner planetary system (∼8000 day baseline; L. Hirsch et al. 2020, in preparation).

We thank the time assignment committee of the University of California for observing time on the Automated Planet Finder for the TESS-Keck Survey. We thank NASA for funding associated with our Key Strategic Mission Support project for TESS–Keck–Survey. We thank Ken and Gloria Levy, who supported the construction of the Levy Spectrometer on the Automated Planet Finder. We thank the University of California and Google for supporting Lick Observatory and the UCO staff for their dedicated work scheduling and operating the telescopes of Lick Observatory. This paper is based on data collected by the TESS mission. Funding for the TESS mission is provided by the NASA Explorer Program. T.D. acknowledges support from MIT's Kavli Institute as a Kavli postdoctoral fellow. M.N.G. acknowledges support from MIT's Kavli Institute as a Torres postdoctoral fellow. P.D. acknowledges support from a National Science Foundation Astronomy and Astrophysics Postdoctoral Fellowship under award AST-1903811. J.M.A.M. gratefully acknowledges support from the National Science Foundation Graduate Research Fellowship under grant No. DGE-1842400. J.M.A.M. also thanks the LSSTC Data Science Fellowship Program, which is funded by LSSTC, NSF Cybertraining grant No. 1829740, the Brinson Foundation, and the Moore Foundation; his participation in the program has benefited this work. M.H.K. acknowledges Allan R. Schmitt for making his light curve examining software LcTools freely available. D.C. was supported by a grant from the John Templeton Foundation. The opinions expressed in this publication are those of the authors and do not necessarily reflect the views of the John Templeton Foundation. S.A. acknowledges the support from the Danish Council for Independent Research through the DFF Sapere Aude Starting grant No. 4181-00487B, and the Stellar Astrophysics Centre which funding is provided by The Danish National Research Foundation (grant agreement No.: DNRF106).

Facilities: Automated Planet Finder (Levy), TESS.

Software: Batman (Kreidberg 2015), Emcee (Foreman-Mackey et al. 2013), EXOFAST (Eastman et al. 2013), Isoclassify (Huber 2017), lmfit(Newville et al. 2014) SpecMatch (Petigura 2015; Yee et al. 2017).

ORCID iDs

Fei Dai https://orcid.org/0000-0002-8958-0683
Arpita Roy https://orcid.org/0000-0001-8127-5775
Benjamin Fulton https://orcid.org/0000-0003-3504-5316
Paul Robertson https://orcid.org/0000-0003-0149-9678
Lea Hirsch https://orcid.org/0000-0001-8058-7443
Howard Isaacson https://orcid.org/0000-0002-0531-1073
Simon Albrecht https://orcid.org/0000-0003-1762-8235
Andrew W. Mann https://orcid.org/0000-0003-3654-1602
Martti H. Kristiansen https://orcid.org/0000-0002-2607-138X
Natalie M. Batalha https://orcid.org/0000-0002-7030-9519
Corey Beard https://orcid.org/0000-0001-7708-2364
Aida Behmard https://orcid.org/0000-0003-0012-9093
Ashley Chontos https://orcid.org/0000-0003-1125-2564
Paul A. Dalba https://orcid.org/0000-0002-4297-5506
Courtney Dressing https://orcid.org/0000-0001-8189-0233
Steven Giacalone https://orcid.org/0000-0002-8965-3969
Michelle Hill https://orcid.org/0000-0002-0139-4756
Andrew W. Howard https://orcid.org/0000-0001-8638-0320
Daniel Huber https://orcid.org/0000-0001-8832-4488
Stephen R. Kane https://orcid.org/0000-0002-7084-0529
Molly Kosiarek https://orcid.org/0000-0002-6115-4359
Jack Lubin https://orcid.org/0000-0001-8342-7736
Andrew Mayo https://orcid.org/0000-0002-7216-2135
Teo Mocnik https://orcid.org/0000-0003-4603-556X
Joseph M. Akana Murphy https://orcid.org/0000-0001-8898-8284
Erik A. Petigura https://orcid.org/0000-0003-0967-2893
Lee Rosenthal https://orcid.org/0000-0001-8391-5182
Ryan A. Rubenzahl https://orcid.org/0000-0003-3856-3143
Lauren M. Weiss https://orcid.org/0000-0002-3725-3058
Judah Van Zandt https://orcid.org/0000-0002-4290-6826
George R. Ricker https://orcid.org/0000-0003-2058-6662
Roland Vanderspek https://orcid.org/0000-0001-6763-6562
David W. Latham https://orcid.org/0000-0001-9911-7388
Sara Seager https://orcid.org/0000-0002-6892-6948
Joshua N. Winn https://orcid.org/0000-0002-4265-047X
Jon M. Jenkins https://orcid.org/0000-0002-4715-9460
Douglas A. Caldwell https://orcid.org/0000-0003-1963-9616
David Charbonneau https://orcid.org/0000-0002-9003-484X
Tansu Daylan https://orcid.org/0000-0002-6939-9211
Maximilian N. Günther https://orcid.org/0000-0002-3164-9086
Edward Morgan https://orcid.org/0000-0003-1447-6344
Samuel N. Quinn https://orcid.org/0000-0002-8964-8377
Mark E. Rose https://orcid.org/0000-0003-4724-745X
Jeffrey C. Smith https://orcid.org/0000-0002-6148-7903

References

Albrecht, S., Winn, J. N., Marcy, G. W., et al. 2013, ApJ, 771, 11
Batygin, K. 2012, Natur, 491, 418
Bryan, M. L., Knutson, H. A., Lee, E. J., et al. 2019, AJ, 157, 52
Choi, J., Dotter, A., Conroy, C., et al. 2016, ApJ, 823, 102
Clanton, C., & Gaudi, B. S. 2014, ApJ, 791, 91

Coelho, P., Barbuy, B., Meléndez, J., Schiavon, R. P., & Castilho, B. V. 2005, A&A, 443, 735
Cumming, A., Butler, R. P., Marcy, G. W., et al. 2008, PASP, 120, 531
Dalal, S., Hébrard, G., Lecavelier des Étangs, A., et al. 2019, A&A, 631, A28
David, T. J., Hillenbrand, L. A., Petigura, E. A., et al. 2016, Natur, 534, 658
Dong, S., Xie, J.-W., Zhou, J.-L., Zheng, Z., & Luo, A. 2018, PNAS, 115, 266
Eastman, J., Gaudi, B. S., & Agol, E. 2013, PASP, 125, 83
Fabrycky, D., & Tremaine, S. 2007, ApJ, 669, 1298
Fang, J., & Margot, J.-L. 2012, ApJ, 761, 92
Foreman-Mackey, D., Hogg, D. W., Lang, D., & Goodman, J. 2013, PASP, 125, 306
Fulton, B. J., & Petigura, E. A. 2018, AJ, 156, 264
Fulton, B. J., Petigura, E. A., Howard, A. W., et al. 2017, AJ, 154, 109
Gaia Collaboration, Brown, A. G. A., Vallenari, A., et al. 2018, A&A, 616, A1
Hirano, T., Suto, Y., Winn, J. N., et al. 2011, ApJ, 742, 69
Howard, A. W., Johnson, J. A., Marcy, G. W., et al. 2010, ApJ, 721, 1467
Huber, D. 2017, Isoclassify: V1.2, vv1.2, Zenodo, doi:10.5281/zenodo.573372
Huber, D., Chaplin, W. J., Christensen-Dalsgaard, J., et al. 2013a, ApJ, 767, 127
Huber, D., Carter, J. A., Barbieri, M., et al. 2013b, Sci, 342, 331
Huber, D., Zinn, J., Bojsen-Hansen, M., et al. 2017, ApJ, 844, 102
Jones, J., White, R. J., Boyajian, T., et al. 2015, ApJ, 813, 58
Kreidberg, L. 2015, PASP, 127, 1161
Lai, D., Foucart, F., & Lin, D. N. C. 2011, MNRAS, 412, 2790
Li, G., Naoz, S., Valsecchi, F., Johnson, J. A., & Rasio, F. A. 2014, ApJ, 794, 131
Mann, A. W., Gaidos, E., Mace, G. N., et al. 2016, ApJ, 818, 46
Mann, A. W., Johnson, M. C., Vanderburg, A., et al. 2020, arXiv:2005.00047
Masuda, K., & Winn, J. N. 2020, AJ, 159, 81
Masuda, K., Winn, J. N., & Kawahara, H. 2020, AJ, 159, 38
Mills, S. M., Howard, A. W., Petigura, E. A., et al. 2019, AJ, 157, 198
Newville, M., Stensitzki, T., Allen, D. B., & Ingargiola, A. 2014, LMFIT: Non-Linear Least-Square Minimization and Curve-Fitting for Python, v0.8.0, Zenodo, doi:10.5281/zenodo.11813
Petigura, E. A. 2015, PhD thesis, Univ. California, Berkeley
Petigura, E. A., Howard, A. W., & Marcy, G. W. 2013, PNAS, 110, 19273
Petigura, E. A., Howard, A. W., Marcy, G. W., et al. 2017, AJ, 154, 107
Ribas, I., Guinan, E. F., Güdel, M., & Audard, M. 2005, ApJ, 622, 680
Ricker, G. R., Winn, J. N., Vanderspek, R., et al. 2014, Proc. SPIE, 9143, 914320
Sanchis-Ojeda, R., Fabrycky, D. C., Winn, J. N., et al. 2012, Natur, 487, 449
Sanchis-Ojeda, R., Winn, J. N., Marcy, G. W., et al. 2013, ApJ, 775, 54
Spalding, C., & Batygin, K. 2015, ApJ, 811, 82
van Eylen, V., & Albrecht, S. 2015, ApJ, 808, 126
Vogt, S. S., Allen, S. L., Bigelow, B. C., et al. 1994, Proc. SPIE, 2198, 362
Vogt, S. S., Radovan, M., Kibrick, R., et al. 2014, PASP, 126, 359
Wang, L., & Dai, F. 2018, ApJ, 860, 175
Winn, J. N., Petigura, E. A., Morton, T. D., et al. 2017, AJ, 154, 270
Wu, Y., & Lithwick, Y. 2011, ApJ, 735, 109
Xie, J.-W., Dong, S., Zhu, Z., et al. 2016, PNAS, 113, 11431
Yee, S. W., Petigura, E. A., & von Braun, K. 2017, ApJ, 836, 77
Yee, S. W., Petigura, E. A., Fulton, B. J., et al. 2018, AJ, 155, 255
Zhu, W., Petrovich, C., Wu, Y., Dong, S., & Xie, J. 2018, ApJ, 860, 101
Zhu, W., & Wu, Y. 2018, AJ, 156, 92